International Journal of Engineering Research & Technology (IJERT)
ISSN: 2278-0181
Vol. 15 Issue 02 , February - 2026

The Effect of Thermo-Diffusion, Thermal Radiation and Radiation Absorption on Convective Heat and Mass Transfer Flow of Micropolar Fluid in A Circular Annulus with Heat Source

Dr. Anjna Singh
Professor, Department of Mathematics, Government Girls P.G. College,
Rewa-486001, Madhya Pradesh, India

Abstract : In this paper, we examine to investigate combined influence of magnetic field and dissipation on connective heat and mass transfer flow of a viscous chemically reacting fluid through a porous medium in the concentric cylindrical annulus with inner cylinder maintained at constant temperature and concentration on the other cylinder maintained constant heat flux. The equations governing the flow, Heat, Mass and micro rotation are solved by employing Galerkin finite element analysis with quadratic approximation functions. The temperature, concentration and micro concentration distributions are analyzed for different values of G, M, D^{-1}, R, S and Ec. The rate of heat and mass transfer and couple stress are numerically evaluated for different variations of the governing parameters.

Keywords : Thermal Radiation, Heat and Mass Transfer, Heat Source, Micro polar fluid, Thermo-diffusion

1. INTRODUCTION:

An enclosed cylindrical annular cavity formed by three vertical, concentric cylinders, containing a fluid through which heat is transferred by natural convection, is a simplified representation of a number of practical and experimental situations. Also, the annulus represents a common geometry employed in a variety of heat transfer systems ranging from simple heat exchangers to the most complicated nuclear reactors. Since, the flow and heat transfer in a cylindrical annular configuration contains all the essential physics that are common to all confined natural convective flows, a complete understanding of the flow in such geometry is very essential. In addition, from a computational stand point, the annular configuration allows investigation of a wide range of geometrical effects. Convection is an important phenomenon in the crystal growth techniques as it can account for heat transfer in the liquid phase and can change the material properties. It has been shown that in order to enhance crystal purity and compositional uniformity, it is necessary to control the transport processes.

There have been widespread interests in the study of effect of magnetic field on natural convection in fluid saturated cylindrical porous annulus/annuli. Most of the studies found in literature on the effect of magnetic field on natural convection are mainly confined to rectangular enclosures or single cylindrical annulus in the presence and absence of porous medium. Several [Sankar and Venkatachalappa [21], Prasad and Kulacki [20], Shivakumara [22], Prasad *et al.* [18], Oreper and Szekely [17], Okada and Ozoe [16] Barletta *et al.* [2], Grosan *et al.* [8] have investigated the effect of direction of magnetic field in a vertical cylindrical annulus.

The theory of micropolar fluids initiated by Erigen [5] exhibits some microscopic effects arising from the local structure and micro motion of the fluid elements. Further, they can sustain couple stress and include classical Newtonian fluid as a special case. The model of micropolar fluid represents fluids consisting of rigid randomly oriented (or Sphenical) particles suspended in a viscous medium where the deformation of the particles is ignored. The fluid containing certain additives, some polymeric fluids and animal blood are examples of micropolar fluids. The mathematical theory of equations of micropolar fluids and application of these fluids in the theory of lubrication and porous media is presented by Lukaszewics [12]. Agarwal and Dhanpal [1] obtained numerical solution of micropolar fluid flow and heat transfer between two co-axial porous circular cylinders.

Panja *et al.* [19] studied the flow of electrically conducting Reiner – Rivlin fluid between two non-conducting co axial circular cylinders with porous walls in the presence of uniform magnetic field. Shivashankar

International Journal of Engineering Research & Technology (IJERT)
ISSN: 2278-0181
Vol. 15 Issue 02 , February - 2026

et al. [23] have obtained numerical solution to the MHD flow of micropolar fluid between two concentric porous cylinders; Murthy *et al.* [14] have considered study flow of micropolar fluid through a circular pipe and transverse with constant suction and injection.

All the above mentioned studies are based on the hypothesis that the effect of dissipation is neglected. This is possible in case of ordinary fluid flow like air and water under gravitational force. But this effect is expected to the relevant for fluids with high values of the dynamic viscosity flows. Moreover, Gebhart [10], Gebhart and Mollendorf [11] have shown that viscous dissipation heat in the natural convective flow is important when the flow field is of extreme size at extremely low temperature or in high gravitational field. On the other hand Barletta [3] have pointed out that relevant effects of viscous dissipation on the temperature profiles and on Nusselt number my occur in the fully developed forced convection in tubes. In view of this several authors notably [Soundalgekar and Pop [26]. Soundalgekar *et al.* [24], Barletta and Zanhicn [4], Sreevani [25], El-Hakein [6] and Barletta [3] Fand and Brucker [7], Giampietrao Fabbn [9] and Sreevani [25], Nakayama and Pop [15]] have studied the effect of viscous dissipation on the convective flows past an infinite vertical plate and through vertical channels and ducts. This observation has been pointed also by Murthy and Singh [13] for the natural connection flow along an isothermal wall embedded in a porous medium. They concluded that e effect of viscous dissipation increases as we move from Non-Darcy regime to Darcy regime. Recently, Sulochana et al(25a) have analysed the effect of dissipation and Soret effect on convective heat and mass transfer flow through a porous medium in a concentric annulus.

2. FORMULATION OF THE PROBLEM

We consider the steady flow of an incompressible, viscous, electrically conducting micropolar fluid through a porous medium in an annulus region between the concentric porous cylinders r = a and r = b (b > a) under the influence of a radial magnetic field $\frac{H_0}{r^2}$.

The fluid is injected through the inner cylinder with radial velocity u_b and flows outward through the outer cylinder with a radial velocity u_a. We also take the viscous, Darcy and Ohmic dissipation into account

The velocity and micro rotation are taken in the form

$v_r = u(r), v_\theta = v = 0, \quad v_z = w(r)$

$\omega_r = 0, \quad \omega_\theta = \omega(r), \quad \omega_z = 0$ (2.1)

The equations governing the flow and heat and mass transfer (2.1)

$$\left.\begin{aligned} &\frac{\partial u}{\partial r}+\frac{u}{r}=0 \\ &\rho u\frac{\partial u}{\partial r}=-\frac{\partial \phi}{\partial r}+(\mu+k)\left(\frac{\partial^2 u}{\partial r^2}+\frac{1}{r}\frac{\partial u}{\partial r}-\frac{u}{r^2}\right)-\left(\frac{\mu}{k_1}\right)u \end{aligned}\right\} \quad (2.2)$$

$$\rho u\frac{\partial w}{\partial r}=-\frac{\partial p}{\partial z}+(\mu+k)\left(\frac{\partial^2 w}{\partial r^2}+\frac{1}{r}\frac{\partial w}{\partial r}\right)-\rho\bar{g}-\left(\frac{\mu}{k_1}\right)w \quad (2.3)$$

$$-k\frac{\partial w}{\partial r}(r\omega)$$

$$\rho j u\frac{\partial \omega}{\partial r}=r\left(\frac{\partial^2 \omega}{\partial r^2}+\frac{1}{r}\frac{\partial \omega}{\partial r}-\frac{N}{r^2}\right)-k\frac{\partial w}{\partial r}-2k\omega \quad (2.4)$$

International Journal of Engineering Research & Technology (IJERT)
ISSN: 2278-0181
Vol. 15 Issue 02 , February - 2026

$$\rho_0 C_p w\frac{\partial T}{\partial z}=k_f\left(\frac{\partial^2 T}{\partial r^2}+\frac{1}{r}\frac{\partial T}{\partial r}\right)+(2\mu+k)\left[\left(\frac{\partial u}{\partial r}\right)^2+\frac{\mu^2}{r^2}+\frac{1}{2}\left(\frac{\partial w}{\partial r}\right)^2\right]$$

$$+2k\left(\frac{1}{2}\frac{\partial w}{\partial r}+\omega\right)^2-2\frac{\beta}{r}\omega\frac{\partial \omega}{\partial r}+r\left(\left(\frac{\partial \omega}{\partial r}\right)^2+\frac{\omega^2}{r^2}\right)-Q_H(T-T_e)+Q_1^{'}(C-C_e)-\frac{1}{r}\frac{\partial(rq_R)}{\partial r}$$

$$+\frac{D_m K_T}{C_s C_p}\left(\frac{\partial^2 C}{\partial r^2}+\frac{1}{r}\frac{\partial C}{\partial r}\right)$$

(2.5)

$$w\frac{\partial C}{\partial z}=D_m\left(\frac{\partial^2 C}{\partial r^2}+\frac{1}{r}\frac{\partial C}{\partial r}\right)-\gamma' C+\frac{D_m K_T}{T_m}\left(\frac{\partial^2 T}{\partial r^2}+\frac{1}{r}\frac{\partial T}{\partial r}\right) \qquad (2.6)$$

$$\rho-\rho_o=-\beta\rho_o(T-T_o)-\beta^{\bullet}\rho_o(C-C_o) \qquad (2.7)$$

where u, w are the velocity components along 0(r, z) directions, T is the temperature, ω is the micro rotation, p is the pressure, ρ is the density, μ is the dynamic viscosity, C_p is the specific heat at constant pressure, k_f is the thermal conductivity, k_1 is the permeability of the porous permeability, σ is the electrical conductivity μ is the magnetic permeability and k, r, β are the material constants.

The boundary conditions are

u = ub, w = 0, ω = 0, T = T_0 + A_0 z , C = C_0 + B_0 z on r = a (2.8)

u = ua, w = 0, ω = 0, T = T_1 + A_0 z , C =C_1 + B_0 z on r = b

From the equation of continuity we obtain

$ru = c$, constant $\Rightarrow ru = au_a = bu_b$

$$\Rightarrow u=\frac{au_a}{r}$$

In view of the boundary condition on temperature and concentration, we may write

T = T_0 + A_0 (z) + θ(r) , C =C_0 + B_0(z) + ϕ(r) (2.10)

Invoking Rosseland approximation(**) the radiative heat flux is

On introducing the non-dimensional variables r′, w′, θ′, p′ and N′ as

$$r'=\frac{r}{a},w'=\frac{w}{\nu/a},\theta=\frac{T-T_0}{T_i-T_0},\omega'=\frac{(\mu+k)\omega}{\rho\left(\mu^2/a^2\right)},p'=\frac{p}{\rho\left(\mu^2/a^2\right)},\phi=\frac{C-C_0}{C_i-C_0} \qquad (2.11)$$

International Journal of Engineering Research & Technology (IJERT)
ISSN: 2278-0181
Vol. 15 Issue 02 , February - 2026

The equations (2.2) – (2.4) reduces to (on dropping the dashes)

$$w_{rr}+\left(1-\frac{S}{1+\Delta}\right)\frac{1}{r}w_r=-\pi_1+\frac{M^2}{r^2}w+D_1^{-1}w-G_1(\theta+N\phi)-\frac{\Delta_1}{r}\frac{\partial}{\partial r}(r\omega)$$

$$\omega_{rr}+(1-SA)\frac{1}{r}\omega_r-\left(\frac{1}{r^2}-\frac{2\Delta}{A}\right)\omega=\frac{\Delta_1}{A\,r}\frac{dw}{dr} \qquad (2.12)$$

$$P_rN_Tw=(1+4Rd/3)\theta_{rr}+\frac{1}{r}\theta_r-\alpha\theta+Q_1\phi+Du\phi_{rr}+$$

$$+EcP_r\left\{\begin{array}{c}(2+\Delta)\left(\frac{S^2}{r^4}+w_r^2\right)+2\Delta\left(\frac{1}{2}w_r+\omega\right)^2\\ -2\Delta\omega\frac{\partial\omega}{\partial r}+A_1\left(w_r^2+\frac{\omega^2}{r^4}\right)\end{array}\right\} \qquad (2.13)$$

$$Sc\,N_cw=\phi_{rr}+\frac{1}{r}\phi_r-\gamma\varphi+ScSo(\theta_{rr}+\frac{1}{r}\theta_r) \qquad (2.14)$$

Where

$G=\frac{\beta g a^3(T_i-T_0)}{\nu^2}$ (Grashof number), $D^{-1}=\frac{a^2}{k_1}$ (Darcy parameter)

$P_r=\frac{\mu C_p}{k_f}$ (Prandtl number), $Ec=\frac{a^2}{C_p(T_i-T_0)\nu^2}$ (Eckert number)

$\alpha=\frac{Q_H a^2}{k_f C_p}$ (Heat source parameter), $S=\frac{au_a}{\nu}$ (Suction parameter)

$So=\frac{D_mK_T(T_i-T_0)}{T_m(C_i-C_0)}$ (Soret parameter), $Du=\frac{D_mK_T(C_i-C_0)}{C_sC_p(T_i-T_0)}$ (Dufour parameter)

$Q_1=\frac{Q_1'(C_i-C_0)a^2}{C_p(T_i-T_0)}$ (Radiation Absorption parameter), $Rd=\frac{4\sigma^{\bullet}T_e^3}{\beta_R k_f}$ (Radiation parameter)

$\gamma=\frac{\gamma' a^2}{D_m}$ (Chemical Reaction parameter), $A=\frac{r}{\mu a^2}$ $\Delta=\frac{\mu}{k}$ (Micropolar parameters)

$\Delta_1=\frac{\Delta}{1+\Delta}$, $D_1^{-1}=\frac{D^{-1}}{1+\Delta}$, $G_1=\frac{G}{1+\Delta}$, $r=\frac{b}{a}$

The non-dimensional boundary conditions are

w = 0,	θ = 1,	ϕ =1	N = 0	on	r = 1
w = 0,	θ = 0,	ϕ =0	N = 0	on	r = s

(2.15)

3. METHOD OF SOLUTION

Finite Element Analysis:

The finite element analysis with quadratic polynomial approximation functions is carried out along the radial distance across the circular cylindrical annulus. The behavior of the velocity, temperature and concentration profiles has been discussed computationally for different variations in governing parameters. The Gelarkin method has been adopted in the variation formulation in each element to obtain the global coupled

International Journal of Engineering Research & Technology (IJERT)
ISSN: 2278-0181
Vol. 15 Issue 02 , February - 2026

matrices for the velocity, temperature and concentration in course of the finite element analysis. Choose an arbitrary element e_k and let w^k, θ^k and N^k be the values of w, θ and N in the element e_k.

We define the error residuals as

$$E_w^k = \frac{d}{dr}\left(r\frac{dw^k}{dr}\right) - \frac{\lambda}{1+\Delta}\frac{dw^k}{dr} + \Delta_1(r\omega^k) + \pi_1 r - D^{-1}rw^k - Gr(\theta^k + N\varphi^k) \tag{2.16}$$

$$\left.\begin{aligned} E_\theta^k = (1+4Rd/3)\frac{d}{dr}\left(r\frac{d\theta^k}{dr}\right) - P_r N_t w_r - \alpha\theta + Du\frac{d}{dr}\left(r\frac{d\phi^k}{dr}\right) + Q_1\phi \\ + EcP_r\left\{\begin{aligned} &(2+\Delta)\frac{\lambda^2}{r^3} + ((2+\Delta)r + A)\left(\frac{dw}{dr}\right)^2 + \\ &2\Delta r\left(\frac{1}{2}\frac{dw}{dr} + \right)^2 \omega - 2A\omega\frac{d\omega}{dr} + A_1\frac{\omega^2}{r} \end{aligned}\right. \end{aligned}\right\} \tag{2.17}$$

$$E_C^k = \frac{d}{dr}\left(r\frac{d\phi^k}{dr}\right) - ScN_C w_r - \gamma\phi^k + ScSo\frac{d}{dr}\left(r\frac{d\phi^k}{dr}\right) \tag{2.18}$$

$$E_N^k = \frac{d}{dr}\left(r\frac{d\omega^k}{dr}\right) - \omega Ar\frac{d\omega^k}{dr} - \left(\frac{1}{r} - \frac{2\Delta r}{A}\right)\omega^k - \frac{\Delta}{A}\frac{dw^k}{dr} \tag{2.19}$$

Where w^k, , θ^k , ϕ^k and ω^k are values of w, θ and ω in the arbitrary element e_k. These are expressed as linear combinations in terms of respective local nodal values.

$$\begin{aligned} w^k &= w_1^k\psi_1^k + w_2^k\psi_2^k + w_3^k\psi_3^k = \sum_{i=1}^{3} w_i^k\psi_i^k \\ \theta^k &= \theta_1^k\psi_1^k + \theta_2^k\psi_2^k + \theta_3^k\psi_3^k = \sum_{i=1}^{3} \theta_i^k\psi_i^k \\ \phi^k &= \phi_1^k\psi_1^k + \phi_2^k\psi_2^k + \phi_3^k\psi_3^k = \sum_{i=1}^{3} \phi_i^k\psi_i^k \\ \omega^k &= \omega_1^k\psi_1^k + \omega_2^k\psi_2^k + \omega_3^k\psi_3^k = \sum_{i=1}^{3} \omega_i^k\psi_i^k \end{aligned} \tag{2.20}$$

Where $\psi_1^k, \psi_2^k, \ldots$ etc are Lagrange's quadratic polynomials.

Following the Gelarkin weighted residual method and integrating by parts (2.16) – (2.19) we obtain

$$\begin{aligned} &\int_{r_A}^{r_B} r\frac{dw^k}{dr}\frac{d\psi_j^k}{dr}dr - \frac{S}{1+\Delta}\int_{r_A}^{r_B}\frac{dw^k}{dr}\psi_j^k dr + \Delta_1 r\int_{r_A}^{r_B}\omega^k\psi_j^k + \pi_1\int_{r_A}^{r_B} r\ \psi_j^k dr - \\ &\int_{r_A}^{r_B} D^{-1}rw^k\psi_j^k - G\int_{r_A}^{r_B} r(\theta^k + N\phi^k)\psi_j^k dr = Q_{2.j}^k + Q_{1.j}^k \end{aligned} \tag{2.21}$$

Where

$$-\theta_{1,J}^k = \left[\left(\frac{dw^k}{dr}\right)\left(r\psi_J^k\right)\right]_{rA} + \left[(\omega^k + \theta^k)\psi_j^k\right]_{rA}$$

$$-\theta_{2,J}^k = \left[\left(\frac{dw^k}{dr}\right)\left(r\psi_J^k\right)\right]_{r_B} + \left[(\omega^k + \theta^k)\psi_J^k\right]_{rB}$$

International Journal of Engineering Research & Technology (IJERT)
ISSN: 2278-0181
Vol. 15 Issue 02 , February - 2026

$$(1+4Rd/3)\int_{r_A}^{r_B} r\frac{d\theta^k}{dr}\frac{d\psi^2}{dr}dr = P_r N_t \int_{r_A}^{r_B} rw^k\psi_j^k dr + R_{2J}^k + R_{1J}^k + \alpha\int_{r_A}^{r_B} r\theta^k\psi_j^k dr +$$

$$EcP_r\left\{\begin{array}{l}(2+\Delta)\int_{r_A}^{r_B}\frac{\lambda^k}{r^3}\psi_j^k dr + [(2+\Delta)r + A]\int_{r_A}^{r_B}\left(\frac{dw^k}{dr}\right)^2\psi_j^k dr + 2\Delta r \\ \int_{r_A}^{r_B}\left(\frac{1}{2}\frac{dw^k}{dr}+\omega^k\right)^2\psi_j^k dr - 2A\int_{r_A}^{r_B}\omega^k\frac{d\omega^k}{dr}\psi_j^k dr + A_1\int_{r_A}^{r_B}\frac{(\omega^k)^2}{r}\psi_j^k dr\end{array}\right\} \quad (2.22)$$

$$+Q_1\int_{r_A}^{r_B} r\phi^k\psi_j^k dr$$

$$\int_{r_A}^{r_B} r\frac{d\phi^k}{dr}\frac{d\psi^2}{dr}dr = ScN_c\int_{r_A}^{r_B} rw^k\psi_j^k dr + U_{2J}^k + U_{1J}^k - \gamma\int_{r_A}^{r_B} r\phi^k\psi_j^k dr + \quad (2.23)$$

$$+Du\,\mathrm{Pr}\int_{r_A}^{r_B} r\frac{d\theta^k}{dr}\frac{d\psi^2}{dr}dr$$

Where

$$-R_{1J}^k = \left(\frac{d\theta^k}{dr}(r\psi_J^k)\right)_{rA} + \left[w^k(r\psi_J^k)\right]_{rA} + \left[\omega^k(r\psi_J^k)\right]_{rA}$$

$$-R_{2J}^k = \left(\frac{d\theta^k}{dr}(r\psi_J^k)\right)_{rB} + \left[w^k(r\psi_J^k)\right]_{rB} + \left[\omega^k(r\psi_J^k)\right]_{rB}$$

$$-U_{1J}^k = \left(\frac{d\phi^k}{dr}(r\psi_J^k)\right)_{rA} + \left[w^k(r\psi_J^k)\right]_{rA} + \left[\omega^k(r\psi_J^k)\right]_{rA}$$

$$-U_{2J}^k = \left(\frac{d\phi^k}{dr}(r\psi_J^k)\right)_{rB} + \left[w^k(r\psi_J^k)\right]_{rB} + \left[\omega^k(r\psi_J^k)\right]_{rB}$$

$$\int_{r_A}^{r_B} r\frac{d\omega^k}{dr}\frac{d\psi_j^k}{dr}dr = SAr\int_{r_A}^{r_B}\frac{d\omega^k}{dr}\psi_j^k dr + \int_{r_A}^{r_B}\left(\frac{1}{r}-\frac{2\Delta r}{A}\right)\omega^k\psi_j^k dr \quad (2.24)$$

$$S_{2j}^k + S_{1j}^k + \frac{\Delta}{A}\int_{r_A}^{r_B}\frac{d\omega^k}{dr}\psi_j^k dr$$

Where $-S_{1J}^k = \left(\left(\frac{d\omega^k}{dr}\right)(r\psi_J^k)\right)_{rA}$, $S_{2J}^k = \left(\left(\frac{d\omega^k}{dr}\right)(r\psi_J^k)\right)_{rB}$

Expressing w^k, θ^k, N^k and ω^k in terms of local nodal values in (2.21) – (2.24) we obtain

International Journal of Engineering Research & Technology (IJERT)
ISSN: 2278-0181
Vol. 15 Issue 02 , February - 2026

$$\left.\begin{aligned}&\sum_{i=1}^{3} w^k \int_{r_A}^{r_B} \frac{d\psi_i^k}{dr}\frac{d\psi_j^k}{dr}dr - \frac{\lambda}{1+\Delta}\sum_{i=1}^{3} w^k \int_{r_A}^{r_B} \frac{d\psi_i^k}{dr}\psi_j^k dr \\ &\quad + \Delta_1 \sum_{i=1}^{3} \omega^k \int_{r_A}^{r_B} r\psi_i^k \psi_j^k dr + \sum_{i=1}^{3} \pi_i \int_{r_A}^{r_B} r\psi_i^k \psi_j^k dr \\ &\text{-D}^{-1}\sum_{i=1}^{3} w^k \int_{r_A}^{r_B} r\psi_i^k \psi_j^k dr \\ &\quad - G_1 \sum_{i=1}^{3} (\theta^k + N\phi^k) \int_{r_A}^{r_B} r\psi_i^k \psi_j^k dr = Q_{2J}^k + Q_{1J}^k\end{aligned}\right\} \tag{2.25}$$

$$\left.\begin{aligned}&(1+4Rd/3)\sum_{i=1}^{3}\theta^k \int_{r_A}^{r_B} r\frac{d\psi_i^k}{dr}\frac{d\psi_j^k}{dr}dr - N_t P_r \sum_{i=1}^{3} w^k \int_{r_A}^{r_B} r\psi_i^k\psi_j^k dr + \alpha\sum_{i=1}^{3}\theta^k\int_{r_A}^{r_B} r\psi_i^k\psi_j^k dr \\ &-EcP_r\left\{\begin{aligned}&(2+\Delta)\sum_{r=1}^{3}\int_{r_A}^{r_B}\frac{\lambda^2}{r^3}\psi_i^k\psi_j^k dr \\ &+\left[(2+\Delta)r + A\right]\sum_{i=1}^{3} w^{k^2}\int_{r_A}^{r_B}\left(\frac{d\psi_i^k}{dr}\right)\psi_j^k dr \\ &+2\Delta r\sum_{i=1}^{3}(w^k+\omega^k)^2\int_{r_A}^{r_B}\left(\frac{1}{2}\frac{d\psi_i^k}{dr}+\omega_i^k\right)^2\psi_j^k dr \\ &-2AN\sum_{i=1}^{3}\omega^k\int_{r_A}^{r_B}\frac{d\psi_i^k}{dr}\psi_j^k dr + A_1\sum_{r=1}^{3}\int_{r_A}^{r_B}\frac{\omega^2}{r}\psi_i^k\psi_j^k dr\end{aligned}\right\}+ \\ &\quad + Q_1\sum_{i=1}^{3}\phi^k\int_{r_A}^{r_B} r\psi_i^k\psi_j^k dr = R_{2J}^k + R_{1J}^k\end{aligned}\right| \tag{2.26}$$

$$\begin{aligned}&\sum_{i=1}^{3}\phi^k\int_{r_A}^{r_B} r\frac{d\psi_i^k}{dr}\frac{d\psi_j^k}{dr}dr - N_c Sc\sum_{i=1}^{3} w^k\int_{r_A}^{r_B} r\psi_i^k\psi_j^k dr - \gamma\sum_{i=1}^{3}\phi^k\int_{r_A}^{r_B} r\psi_i^k\psi_j^k dr + \\ &+ScSo\sum_{i=1}^{3}\theta^k\int_{r_A}^{r_B} r\frac{d\psi_i^k}{dr}\frac{d\psi_j^k}{dr}dr_r = U_{2J}^k + U_{1J}^k\end{aligned} \tag{2.27}$$

$$\begin{aligned}&\sum_{i=1}^{3}\omega^k\int_{r_A}^{r_B} r\frac{d\psi_i^k}{dr}\frac{d\psi_j^k}{dr}dr - SA\sum_{i=1}^{3}\omega^k\int_{r_A}^{r_B} r\frac{d\psi_i^k}{dr}\psi_j^k dr \\ &-\sum_{i=1}^{3}\omega^k\int_{r_A}^{r_B}\left(\frac{1}{r}-\frac{2\Delta r}{A}\right)\psi_i^k\psi_j^k dr - \frac{\Delta}{A}\sum_{r=1}^{3} w^k\int_{r_A}^{r_B}\frac{d\psi_i^k}{dr}\psi_i^k dr = S_{2J}^k + S_{1J}^k\end{aligned} \tag{2.28}$$

Choosing different Ψ_j^k's corresponding to each element e_k in the equation (2.25) yields a local stiffness matrix of order 3×3 in the form

$$\begin{aligned}&\left(f_{iJ}^k\right)\left(w_i^k\right) - \delta G_1\left(g_{ij}^k\right)\left(\theta_i^k + N\phi_i^k\right) + \delta D_1^{-1}\left(m_{iJ}^k\right)\left(u_i^k\right) \\ &\quad + \delta^2 A\left(n_{iJ}^k\right)\left(u_i^k\right) = \left(Q_{2J}^k\right) + \left(Q_{1J}^k\right) + \left(v_j^k\right)\end{aligned} \tag{2.29}$$

International Journal of Engineering Research & Technology (IJERT)
ISSN: 2278-0181
Vol. 15 Issue 02 , February - 2026

Likewise the equation (2.26) - (2.28) gives rise to stiffness matrices

$$(1+4Rd/3)\left(e_{iJ}^{k}\right)\left(\theta_{i}^{k}\right)-N_{t}P_{r}\left(t_{iJ}^{k}\right)\left(w_{i}^{k}\right)+\alpha\left(s_{iJ}^{k}\right)\left(\theta_{i}^{k}\right)+Q_{1}\left(p_{iJ}^{k}\right)\left(\phi_{i}^{k}\right)+Du\left(O_{iJ}^{k}\right)\left(\phi_{i}^{k}\right)=R_{2J}^{k}+R_{1J}^{k} \quad (2.30)$$

$$\left(h_{iJ}^{k}\right)\left(\phi_{i}^{k}\right)-N_{c}Sc\left(j_{iJ}^{k}\right)\left(w_{i}^{k}\right)-\gamma\left(k_{iJ}^{k}\right)\left(\phi_{i}^{k}\right)+ScSo\left(O_{iJ}^{k}\right)\left(\theta_{i}^{k}\right)=U_{2J}^{k}+U_{1J}^{k} \quad (2.31)$$

$$\left(l_{iJ}^{k}\right)\left(\omega_{i}^{k}\right)-N_{2}C\left(t_{iJ}^{k}\right)\left(w_{i}^{k}\right) \quad (2.32)$$

Where

$\left(f_{iJ}^{k}\right),\left(g_{iJ}^{k}\right),\left(m_{iJ}^{k}\right),\left(n_{iJ}^{k}\right),\left(e_{iJ}^{k}\right),\left(l_{iJ}^{k}\right),\left(p_{iJ}^{k}\right),\left(t_{iJ}^{k}\right),\left(h_{iJ}^{k}\right),\left(j_{iJ}^{k}\right),\left(k_{iJ}^{k}\right)$ and $\left(O_{iJ}^{k}\right)$ are 3×3 matrices and $V_{j}^{k}=-P_{1}\int_{rA}^{rB}r\psi_{i}^{k}\psi_{j}^{k}dr$ and $\left(Q_{2J}^{k}\right),\left(Q_{1J}^{k}\right),\left(R_{2J}^{k}\right),\left(R_{1J}^{k}\right),\left(S_{2J}^{k}\right)$ and $\left(S_{1J}^{k}\right)$ are 3×1 column matrices and such stiffness (2.29) – (2.32) in terms of local nodes in each element are assembled using inter element continuity and equilibrium conditions to obtain the coupled global matrices in terms of the global nodal values of w, θ, ϕ and ω. In case we choose n-quadratic elements then the global matrices are of order 2n+1. The ultimate coupled global matrices are solved to determine the unknown global nodal values of the velocity, temperature and concentration in fluid region. In solving these global matrices an iteration procedure has been adopted to include the boundary and effects in the porous region.

To evaluate (2.24) to begin with choose the initial global nodal values of w_i's as zeros in the zeroth approximation, we evaluate w_i's, θ_i's, ϕ_i's and ω_i's in the usual procedure mentioned earlier. Later choosing these values of w_i's as first order approximation calculate θ_i's ϕ_i's and ω_i's. In the second iteration, we substitute for w_i's the first order approximation. This procedure is repeated till the consecutive values of w_i's, θ_i's, ϕ_i's and ω_i's differ by a pre-assigned percentage. For computational purpose we choose five elements in flow region.

The shear stress (τ) is evaluated using the formula $\tau=\left(\frac{du}{dr}\right)_{r=1,S}$

The rate of heat transfer (Nusselt number) is evaluated using the formula $Nu=-\left(\frac{d\theta}{dr}\right)_{r,S}$

The rate of mass transfer (Sherwood number) is evaluated using the formula $Sh=-\left(\frac{d\phi}{dr}\right)_{r,S}$

The couple stress at the inner and outer cylinder are evaluated by $M^{*}=-\left(\frac{d\omega}{dr}\right)_{r,S}$

4. COMPARISON

In the absence of Heat sources (α=0), Radiation parameter(Rd=0) and Radiation absorption (Q1=0) the results are in good agreement with those of *Sulochana et al* (25a)

					Sulochana et al(25a)				Present results(α=0,Q1=0,Rd=0)			
N	Ec	γ	Δ	λ	Nu(1)	Nu(2)	Sh(1)	Sh(2)	Nu(1)	Nu(2)	Sh(1)	Sh(2)
1	0.01	0.5	1	0.1	2.8636	-5.1236	4.2065	-10.781	2.8632	-5.1237	4.2068	-10.780
2	0.01	0.5	1	0.1	6.4175	-11.548	6.7759	-15.409	6.4173	-11.546	6.7756	-15.408
-0.5	0.01	0.5	1	0.1	-0.8592	-1.5012	1.7038	-2.6098	-0.8591	-1.5011	1.7036	-2.6096
-1.5	0.01	0.5	1	0.1	0.1787	-0.01638	-0.9098	-1.5997	0.1779	-0.01633	-0.9099	-1.5994
1	0.03	0.5	1	0.1	1.8355	-2.3072	4.2058	-10.7794	1.8356	-2.3071	4.2055	-10.7796
1	0.05	0.5	1	0.1	2.8756	-5.1236	4.2065	-10.8802	2.8754	-5.1233	4.2066	-10.9801
1	0.01	1.5	1	0.1	2.8853	-5.1777	2.2232	-8.7041	2.8857	-5.1774	2.2229	-8.7042
1	0.01	0.5	3	0.1	1.778	-5.2273	1.5148	-5.5912	1.779	-5.2271	1.5149	-5.5911
1	0.01	0.5	5	0.1	1.035	-5.0836	4.0588	-8.4699	1.033	-5.0833	4.0589	-8.4696
1	0.01	0.5	1	0.3	2.8636	-2.8052	2.0811	-6.5156	2.8633	-2.8051	2.0810	2.8636
1	0.01	0.5	1	0.5	2.9613	-5.1236	2.4047	-9.5098	2.9611	-5.1233	2.4049	-9.5099

International Journal of Engineering Research & Technology (IJERT)
ISSN: 2278-0181
Vol. 15 Issue 02 , February - 2026

5. RESULTS AND DISCUSSION:

In this analysis we investigate the effect of thermo-diffusion, diffusion-thermo, dissipation ,Heat sources and chemical reaction on mixed convective heat and mass transfer flow of a micro polar fluid through a porous medium in circular annulus between the cylinders r=a and r=b which are maintained at constant temperature and concentration. The non-linear coupled equations governing the flow heat and mass transfer are solved by Galerkin finite element analysis with quadratic approximation functions. The Prandtl number Pr, material constants A and λ are taken to be constant at 0.733, 1 and 1 respectively where as the effect of other important parameters namely micro polar parameter Δ, the suction Reynolds number λ, Grashof number G, buoyancy ratio N, Magnetic parameter M, Inverse Darcy parameter D^{-1} ,Soret parameter So ,radiation parameter Rd, radiation absorption parameter Q1 and Schmidt number Sc has been studied for these functions and corresponding profiles are shown in Figs. 1, 5, 9, 14, 18, 22 and 26.

Fig. 2a represents the variation of the velocity function (w) with Grashof number G and M The actual axial velocity w is in the vertically downward direction and $w < 0$ represents the actual flow. Therefore, $w > 0$ represents the reversal flow. We notice from the profiles that the magnitude of w enhances with increase in G .The maximum of |w| occurs at r=1.6. The variation of w with M shows that the velocity reduces with increase in M.Thus higher the Lorentz force smaller the velocity in the flow region.Fig. 4a represents w with Darcy parameter D^{-1} and Sc. It is found that lesser the permeability of porous medium (D-1) smaller |w| in the flow region.. The variation of w with Schmidt nu8mber Sc shows that lesser the molecular diffusivity lesser the axial velocity in the flow region.. When the molecular buoyancy force dominates over the thermal force |w| enhances irrespective of the directions of the buoyancy forces in the flow region(fig.4a).Fig.5a represents the variation of w with Soret parameter So and radiation absorption parameter Q1.It can be seen from the graphs that increasing Soret parameter So leads to a depreciation in |w|.Also higher the radiation absorption effects smaller the magnitude of w.The variation of w with heat source parameter α is exhibited in fig.7a..It can be seen from the profiles that higher the strength of the heat generating/absorption source smaller the magnitude of w in the flow region.This is due to the fact that the thermal energy is absorbed in the boundary layer which leads to a deprecation in the axial velocity.Fig. 6a represents w with chemical reaction parameter γ. It is found that the magnitude of w enhances in the generating chemical reaction case and reduces in the degenerating case.Fig.8a represents w with radiation parameter Rd.It can be seen from the profiles that an increase in Rd enhances the magnitude of w in the flow region.The effect of dissipation on w is exhibited in Fig.9a. It is found that higher the dissipative effect(Ec) smaller the axial velocity in the flow region..From fig.10a we find that lesser the thermal diffusivity smaller the magnitude of w in the flow region. Fig.11 represents w with micropolar parameter(Δ).It can be seen from the profiles that the axial velocity depreciates with increase in Δ in the entire flow region. Fig.12a represents w with suction parameter λ.It is found that |w| enhances with increase in λ reduces the axial velocity.An increase in the micropolar parameter (A) decreases the magnitude of w in the flow region(fig.12a).

The non-dimensional temperature (θ) is exhibited in Figs.2b-12b for different parametric values. It is found that the non-dimensional temperature is always positive for all variations. This indicates the actual temperature is always greater than T_0. Fig. 2b represents θ with Grashof number G and magnetic parameter M. It is found that the actual temperature reduces with increase in G, with maximum occurring at r=1. Fig.3b represents θ with D^{-1} and Sc. It can be seen from the profiles that the actual temperature reduces with increase in D^{-1}. Thus lesser the permeability of the porous medium smaller the actual temperature in the flow region. With respecto Sc,we find that lesser the molecular diffusivity smaller the temperature in the flow region. Fig.4b represents θ with buoyancy ratio N. It can be seen from the profiles that the when molecular buoyancy force dominates over the thermal buoyancy force smaller the actual temperature irrespective of the diurections of the buoyancy forces. Higher the thermo-diffusion effects smaller the actual temperature in the flow region(fig.5b)..Fig.7b represents θ with heat source parameter α.We notice from the profiles that the actual temperature enhances with increase in the strength of the heat generating/absorbing source. Fig.6b represents θ with chemical reaction parameter γ. It is found that the actual temperature reduces in the degenerating chemical reaction case and enhances in the generating case.Fig.5b shows the variation of temperature with radiation absorption parameter Q1.We find from the profiles that the actual temperature reduces with increase in Q1.The variation of θ with Eckert number Ec is shown in the Fig. 9b. It is found that the actual temperature reduces with Ec in the entire flow region.Thus higher the dissipation smaller the actual temperature in the flow region.Fig.8b represents θ with radiation parameter Rd.We find that the actual temperature enhances with higher radiative heat flux.From fig.7b we find that the actual temperature enhances with increase in the strength of the heat generating/absorbing heat source.Fig.10b shows the variation of θ with Prandtl number Pr.We find from the profiles that lesser the thermal diffusivity smaller the actual temperature.Fig.11b shows the variation θ with micropolar parameter Δ.Higher the values of Δ,larger the actual temperature in the flow region. The variation of θ with λ is exhibited in Fig.12b. It is found that the actual temperature experiences an enhancement with

International Journal of Engineering Research & Technology (IJERT)
ISSN: 2278-0181
Vol. 15 Issue 02 , February - 2026

increase in suction parameter λ in the flow region.Fig.12b exhibits θ with micropolar parameter A.It can be seen from the graphs that the actual temperature reduces with higher A.

The concentration distribution (C) is exhibited in Figs.2c-16c. We follow the convention that the non-dimensional concentration distribution is positive or negative according as the actual concentration is greater/lesser than C_0. Fig. 2c represents the concentration with G and M. It is found that the actual concentration enhances with increase in G. Higher the Lorentz force (M) larger the actual concentration Fig. 3c represents C with D^{-1} and Sc. Lesser the permeability of the porous medium(D^{-1}) larger the actual concentration in the flow region. The variation of concentration C with Sc shows that lesser the molecular diffusivity(Sc) larger the actual concentration the actual concentration in the flow region. The variation of C with buoyancy ratio(N) is shown in fig.4c.It can be seen from the profiles that when the molecular buoyancy force dominates over the thermal buoyancy force the actual concentration enhances irrespective of the directions of the buoyancy forces. Fig.5c shows the variation of C with Soret parameter So . In can be seen from the profiles that higher the thermo-diffusion effects larger the actual concentration in the flow region. The variation of C with Q1shows that the actual concentration increases with Q1(fig.5c).From fig.6c we find that the actual concentration experiences an enhancement in the generating chemical reaction case ($\gamma<0$) and in degenerating chemical reaction case ($\gamma>0$) it reduces in the flow region.The variation of C with Eckert number Ec is exhibited in fig.9c.Higher the dissipative energy smaller the actual concentration in the flow region.The variation of concentration with heat source parameter α is shown in Fig. 7c. It is found that higher the strength of the heat generating/absorbing source lesser the actual temperature in the flow region.. The variation of C with Rd shows that higher the radiative heat flux larger the actual concentration in the flow region(fig.8c).Lesser the thermal diffusivity smaller the actual concentration (fig.10c).The actual concentration reduces with increase in micropolar parameters,Δ (fig.11c) .An increase in A reduces the actual concentration The variation of θ with λ is exhibited in Fig.12c. It is found that the actual concentration experiences an enhancement with increase in suction parameter(λ).

The micro rotation (ω) is shown in Figs.2d-15d for different parametric values. Fig. 2d represents ω with Grashof number G and M. It is found that the magnitude of ω enhances with G, maximum occurring at r=1.5. Higher the Lorentz force(M) larger the micro-rotation .Fig.3c represents ω with D^{-1} and Sc. It is found Lesser the permeability of the porous medium smaller the magnitude of the micro-rotation. We notice a depreciation in |ω| with increase in Sc. Fig. 4d represents ω with buoyancy ratio N. It is found that the magnitude of ω decreases in the region($1\le r\le 1.5$) and enhances in the region($1.6\le r\le 1.95$) with increase in N>0 when the buoyancy forces are in the same direction and for the forces acting in opposite directions,it depreciates in the flow region. Higher the thermo-diffusion effects(So) smaller the magnitude of the angular velocity in the region($1\le r\le 1.5$) and larger the magnitude of the angular velocity in the flow region ($1.6\le r\le 1.95$). Higher the radiation absorption effects larger the magnitude of the micro-rotation(fig.5d).From fig.6d we notice that the angular velocity ω reduces in the flow region($1\le r\le 1.5$) and enhances in the region ($1.6\le r\le 1.95$) in the degenerating chemical reaction case ($\gamma>0$)and reduces in the generating chemical reaction case($\gamma<0$). From fig.9d we find that higher the dissipation (Ec) larger the micro-rotation in the flow region($1.0\le r\le 1.5$) and reduces in the remaining region.Fig.7d represents ω with heat source parameter α.From the profiles we find that |ω| decreases with increase in the strength of the heat generating/absorbing source in the flow region,Fig.8d shows the variation of ω with radiation parameter Rd.It can be seen from the profiles that higher the radiative heat flux smaller the magnitude of the micro-rotation in the flow region.Fig.10d shows that variation of |ω| with Pr.Lesser the thermal diffusivity larger the angular velocity in the flow region($1.0\le r\le 1.5$) and reduces in the region ($1.6\le r\le 1.95$).An increase in micropolar parameter Δ diffusivity smaller the angular velocity in the flow region($1.0\le r\le 1.5$) and enhances in the region ($1.6\le r\le 1.95$).An increase in suction parameter λ larger the angular velocity in the flow region($1.0\le r\le 1.5$) and smaller in the region ($1.6\le r\le 1.95$).The variation with reference to A shows that |ω| enhances with increase in micropolar parameter A in the flow region(fig.12d).

The stress (τ) at the inner and outer cylinders is exhibited in Tables 2&3 for different parametric values. It is found that τ enhances with increase in G at r=1 and 2. Lesser the permeability of the porous medium/higher the Lorentz force/higher the suction parameter λ smaller τ at both the cylinders.An increase in buoyancy ratio(N) reduces at r=1 and r=2 irrespective of the directions of the buoyancy forces.The stress reduces at r=1 and r=2 with increase in strength of heat generating/absorbibg heat source. Lesser the molecular diffusivity(Sc) larger the stress at both the cylinders.Also lesser the thermal diffusivity larger the stress at r=1 and r=2.An increase in micro rotation parameter A ,results in an enhancement in |τ| at r=2 and depreciation at r=1. With respect to viscosity ratio parameter Δ we find that |τ| reduces at r=1 and r=2.With reference to Eckert number Ec it can be seen that |τ| reduces with increase in Ec at r=1&2.. The variation of τ with chemical reaction parameter γ shows that |τ| enhances at r=1 and r=2 in the generating chemical reaction case and enhances at both the cylinders in the degenerating chemical reaction case.Higher the thermo-diffusivity(So)/radiation absorbing effects larger the stress at both the cylinders.Higher the radiative heat flux smaller the stress at the cylinders.

International Journal of Engineering Research & Technology (IJERT)
ISSN: 2278-0181
Vol. 15 Issue 02 , February - 2026

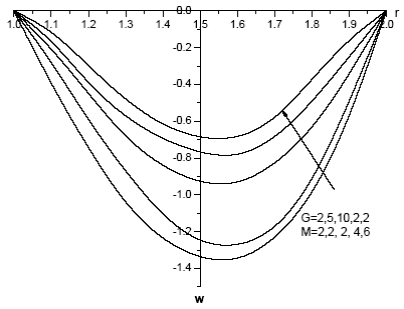

Fig. 2a : Variation of *w* with G & M
D^{-1}=0.2,Sc=0.24, N=1, S_0 =0.5,Q_1=0.5, γ=0.5,α=2,
Ec=0.01, Pr=0.71, Δ=1, λ=0.03, A=1,Rd=0.5

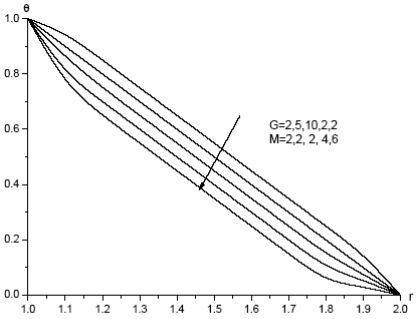

Fig. 2b : Variation of θ with G & M
D^{-1}=0.2,Sc=0.24, N=1, S_0 =0.5,Q_1=0.5, γ=0.5,α=2,
Ec=0.01, Pr=0.71, Δ=1, λ=0.03, A=1,Rd=0.5

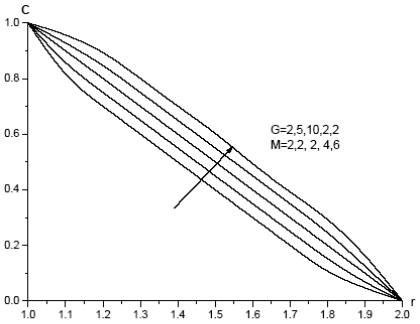

Fig. 2c : Variation of *C* with G & M
D^{-1}=0.2,Sc=0.24, N=1, S_0 =0.5,Q_1=0.5, γ=0.5,α=2,
Ec=0.01, Pr=0.71, Δ=1, λ=0.03, A=1,Rd=0.5

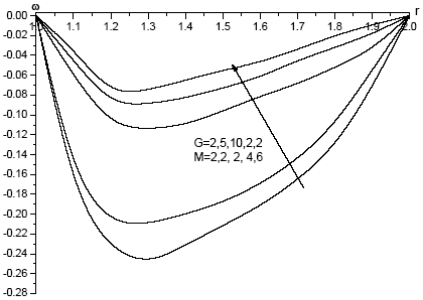

Fig. 2d : Variation of *ω* with G & M
D^{-1}=0.2,Sc=0.24, N=1, S_0 =0.5,Q_1=0.5, γ=0.5,α=2,
Ec=0.01, Pr=0.71, Δ=1, λ=0.03, A=1,Rd=0.5

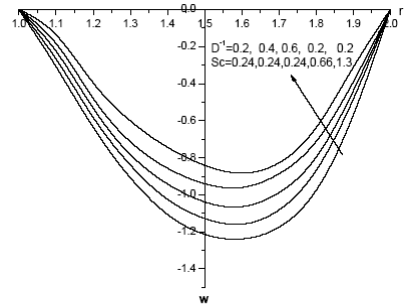

Fig. 3a : Variation of *w* with D^{-1} & Sc
G&M=2, N=1, S_0 =0.5,Q_1=0.5, γ=0.5,α=2,
Ec=0.01, Pr=0.71, Δ=1, λ=0.03, A=1,Rd=0.5

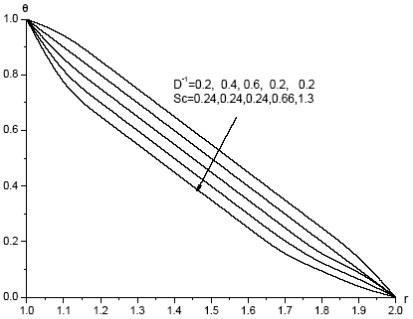

Fig. 3b : Variation of θ with D^{-1} & Sc
G&M=2, N=1, S_0 =0.5,Q_1=0.5, γ=0.5,α=2,
Ec=0.01, Pr=0.71, Δ=1, λ=0.03, A=1,Rd=0.5

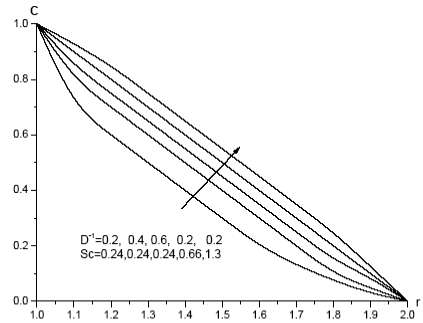

Fig. 3c : Variation of *C* with D^{-1} & Sc
G&M=2, N=1, S_0 =0.5,Q_1=0.5, γ=0.5,α=2,
Ec=0.01, Pr=0.71, Δ=1, λ=0.03, A=1,Rd=0.5

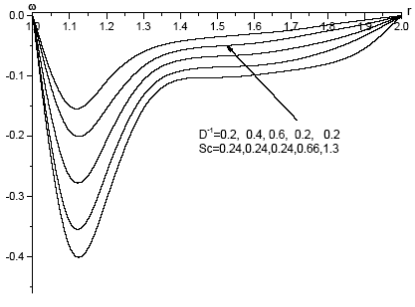

Fig. 3d : Variation of *ω* with D^{-1} & Sc
G&M=2, N=1, S_0 =0.5,Q_1=0.5, γ=0.5,α=2,
Ec=0.01, Pr=0.71, Δ=1, λ=0.03, A=1,Rd=0.5

International Journal of Engineering Research & Technology (IJERT)
ISSN: 2278-0181
Vol. 15 Issue 02 , February - 2026

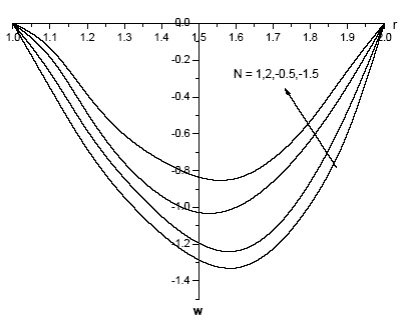

Fig. 4a : Variation of w with N
G&M=2, D^{-1}=0.2,Sc=0.24, S_0=0.5,Q_1=0.5, γ=0.5,α=2,
Ec=0.01, Pr=0.71, Δ=1, λ=0.03, A=1,Rd=0.5

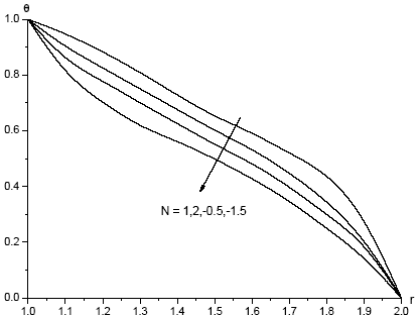

Fig. 4b : Variation of θ with N
G&M=2, D^{-1}=0.2,Sc=0.24, S_0=0.5,Q_1=0.5, γ=0.5,α=2,
Ec=0.01, Pr=0.71, Δ=1, λ=0.03, A=1,Rd=0.5

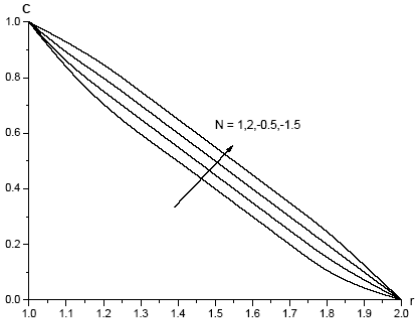

Fig. 4c : Variation of C with N
G&M=2, D^{-1}=0.2,Sc=0.24, S_0=0.5,Q_1=0.5, γ=0.5,α=2,
Ec=0.01, Pr=0.71, Δ=1, λ=0.03, A=1,Rd=0.5

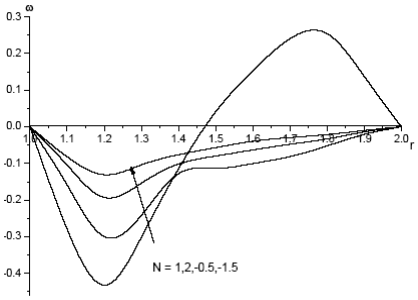

Fig. 4d : Variation of ω with N
G&M=2, D^{-1}=0.2,Sc=0.24, S_0=0.5,Q_1=0.5, γ=0.5,α=2,
Ec=0.01, Pr=0.71, Δ=1, λ=0.03, A=1,Rd=0.5

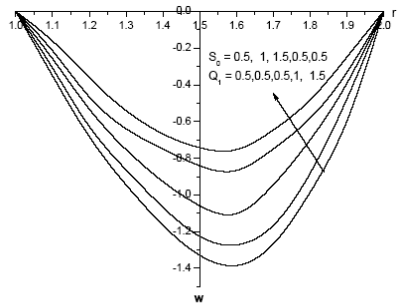

Fig. 5a : Variation of w with S_0 & Q_1
G&M=2, D^{-1}=0.2,Sc=0.24, N=1, γ=0.5,α=2,
Ec=0.01, Pr=0.71, Δ=1, λ=0.03, A=1,Rd=0.5

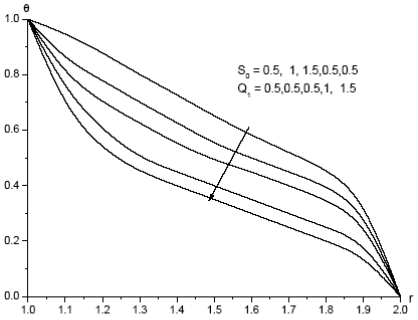

Fig. 5b : Variation of θ with S_0 & Q_1
G=2,M=2, D^{-1}=0.2,Sc=0.24, N=1, γ=0.5,α=2,
Ec=0.01, Pr=0.71, Δ=1, λ=0.03, A=1,Rd=0.5

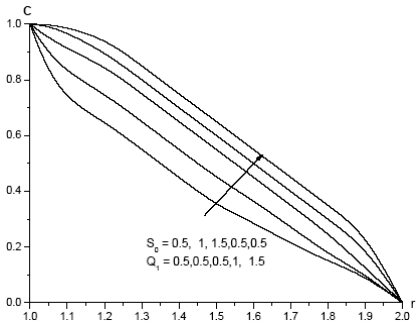

Fig. 5c : Variation of C with S_0 & Q_1
G=2,M=2, D^{-1}=0.2,Sc=0.24, N=1, γ=0.5,α=2,
Ec=0.01, Pr=0.71, Δ=1, λ=0.03, A=1,Rd=0.5

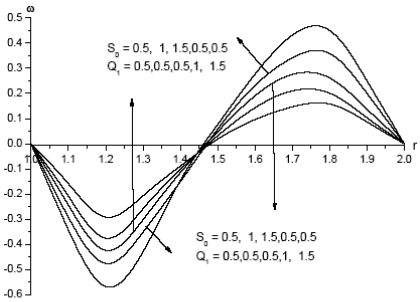

Fig. 5d : Variation of ω with S_0 & Q_1
G=2,M=2, D^{-1}=0.2,Sc=0.24, N=1, γ=0.5,α=2,
Ec=0.01, Pr=0.71, Δ=1, λ=0.03, A=1,Rd=0.5

International Journal of Engineering Research & Technology (IJERT)
ISSN: 2278-0181
Vol. 15 Issue 02 , February - 2026

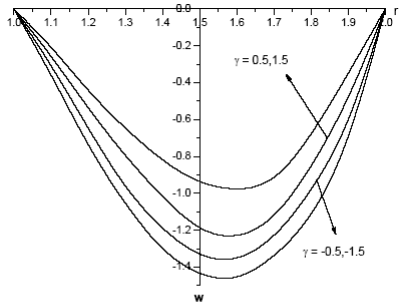

Fig. 6a : Variation of w with γ
G=2,M=2, D^{-1}=0.2,Sc=0.24, N=1, S_0 =0.5,Q_1=0.5, α=2,
Ec=0.01, Pr=0.71, Δ=1, λ=0.03, A=1,Rd=0.5

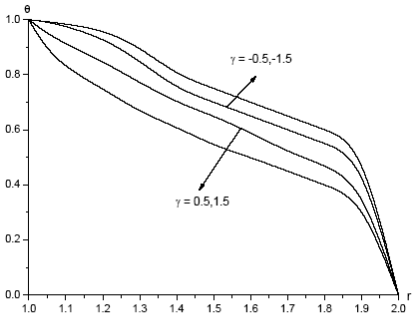

Fig. 6b : Variation of θ with γ
G=2,M=2, D^{-1}=0.2,Sc=0.24, N=1, S_0 =0.5,Q_1=0.5, α=2,
Ec=0.01, Pr=0.71, Δ=1, λ=0.03, A=1

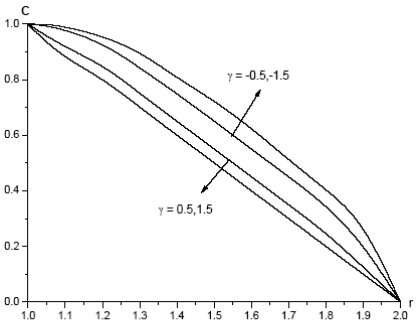

Fig. 6c : Variation of C with γ
G=2,M=2, D^{-1}=0.2,Sc=0.24, N=1, S_0 =0.5,Q_1=0.5,α=2,
Ec=0.01, Pr=0.71, Δ=1, λ=0.03, A=1,Rd=0.5

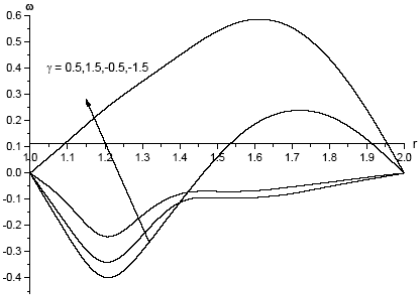

Fig. 6d : Variation of ω with γ
G=2,M=2, D^{-1}=0.2,Sc=0.24, N=1, S_0 =0.5,Q_1=0.5,α=2,
Ec=0.01, Pr=0.71, Δ=1, λ=0.03, A=1,Rd=0.5

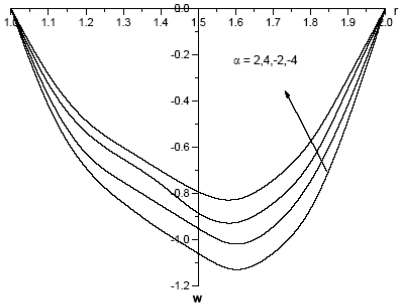

Fig. 7a : Variation of w with α
G=2,M=2, D^{-1}=0.2,Sc=0.24, N=1, S_0 =0.5,Q_1=0.5, γ=0.5,
Ec=0.01, Pr=0.71, Δ=1, λ=0.03, A=1,Rd=0.5

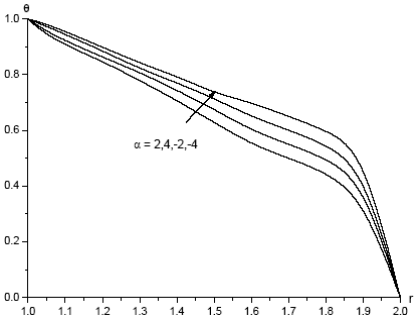

Fig. 7b : Variation of θ with α
G=2,M=2, D^{-1}=0.2,Sc=0.24, N=1, S_0 =0.5,Q_1=0.5, γ=0.5,
Ec=0.01, Pr=0.71, Δ=1, λ=0.03, A=1,Rd=0.5

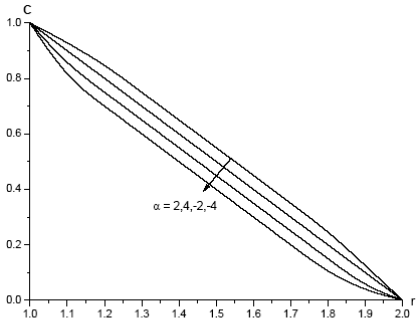

Fig. 7c : Variation of C with α
G=2,M=2, D^{-1}=0.2,Sc=0.24, N=1, S_0 =0.5,Q_1=0.5, γ=0.5,
Ec=0.01, Pr=0.71, Δ=1, λ=0.03, A=1,Rd=0.5

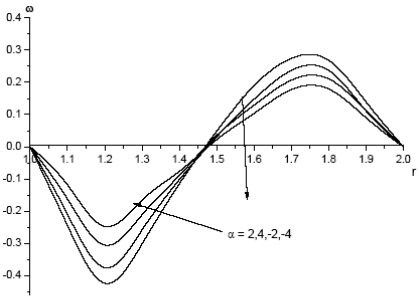

Fig. 7d : Variation of ω with α
G=2,M=2, D^{-1}=0.2,Sc=0.24, N=1, S_0 =0.5,Q_1=0.5, γ=0.5,
Ec=0.01, Pr=0.71, Δ=1, λ=0.03, A=1,Rd=0.5

International Journal of Engineering Research & Technology (IJERT)
ISSN: 2278-0181
Vol. 15 Issue 02 , February - 2026

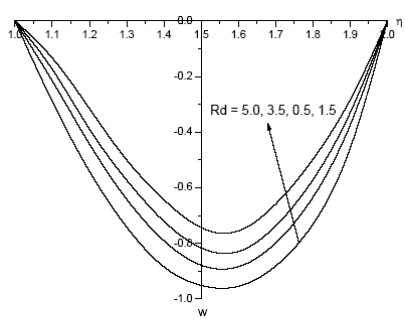

Fig. 8a : Variation of *w* with Rd
G=2, D^{-1}=0.2, N=1, Sc=1.3, Sr&Du=2/0.03, α=2, γ=0.5, Ec=0.01, Δ=0.5, λ=0.3, A=0.5

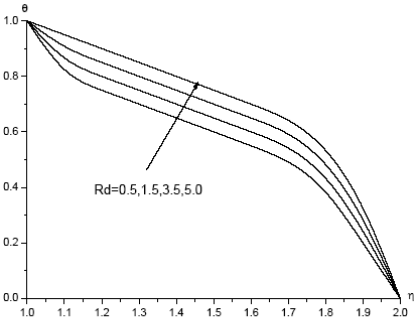

Fig. 8b : Variation of θ with Rd
G=2, D^{-1}=0.2, N=1, Sc=1.3, Sr&Du=2/0.03, α=2, γ=0.5, Pr=0.71, Δ=0.5, λ=0.3, A=0.5

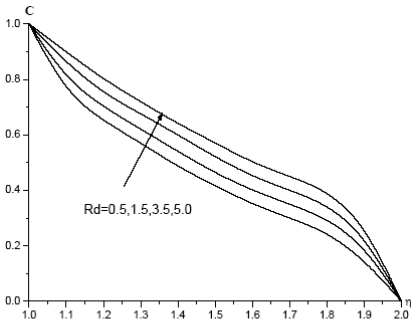

Fig. 8c : Variation of C with Rd
G=2, M=5,D^{-1}=0.2, N=1, Sc=1.3, Sr&Du=2/0.03, α=2, γ=0.5, Ec=0.01, Δ=0.5, λ=0.3, A=0.5

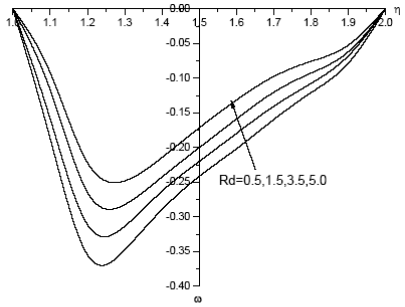

Fig. 8d : Variation of ω with Rd
G=2, M=5,D^{-1}=0.2, N=1, Sc=1.3, Sr&Du=2/0.03, α=2, γ=0.5, Ec=0.01, Δ=0.5, λ=0.3, A=0.5

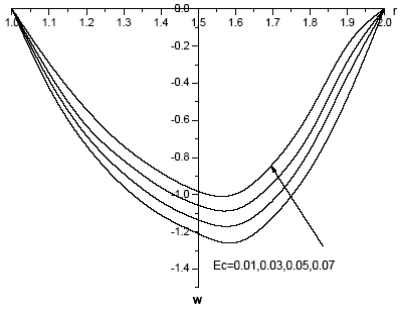

Fig. 9a : Variation of *w* with Ec
G=2,M=2, D^{-1}=0.2,Sc=0.24, N=1, S_0=0.5,Q_1=0.5, γ=0.5,α=2, Pr=0.71, Δ=1, λ=0.03, A=1,Rd=0.5

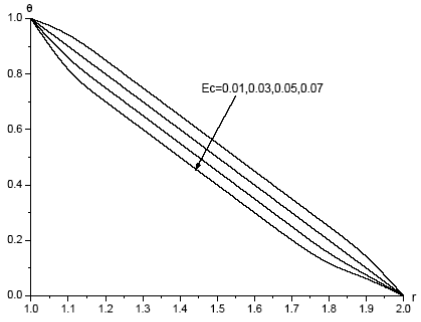

Fig.9b : Variation of θ with Ec
G=2,M=2, D^{-1}=0.2,Sc=0.24, N=1, S_0=0.5,Q_1=0.5, γ=0.5,α=2, Pr=0.71, Δ=1, λ=0.03, A=1,Rd=0.5

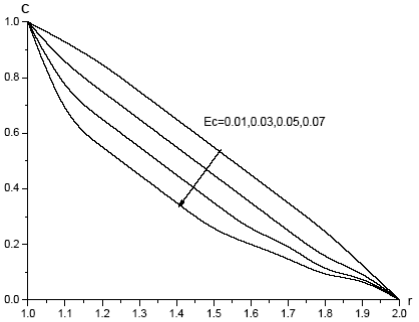

Fig. 9c : Variation of *C* with Ec
G=2,M=2, D^{-1}=0.2,Sc=0.24, N=1, S_0=0.5,Q_1=0.5, γ=0.5,α=2, Pr=0.71, Δ=1, λ=0.03, A=1,Rd=0.5

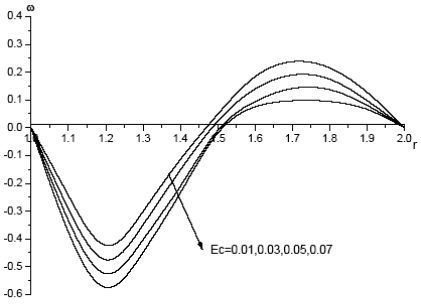

Fig. 9d : Variation of *ω* with Ec
G=2,M=2, D^{-1}=0.2,Sc=0.24, N=1, S_0=0.5,Q_1=0.5, γ=0.5,α=2, Pr=0.71, Δ=1, λ=0.03, A=1,Rd=0.5

International Journal of Engineering Research & Technology (IJERT)
ISSN: 2278-0181
Vol. 15 Issue 02 , February - 2026

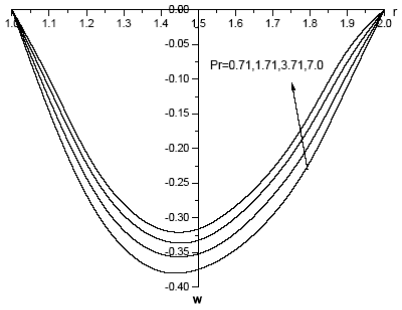

Fig.10a : Variation of w with Pr
G=2,M=2, D^{-1}=0.2,Sc=0.24, N=1, S_0=0.5,Q_1=0.5,
γ=0.5,α=2, Ec=0.01, 9 Δ=1, λ=0.03, A=1,Rd=0.5

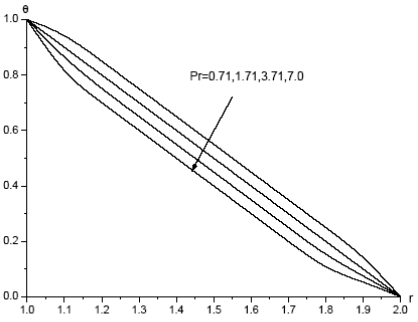

Fig. 10b : Variation of θ with Pr
G=2,M=2, D^{-1}=0.2,Sc=0.24, N=1, S_0=0.5,Q_1=0.5,
γ=0.5,α=2, Ec=0.01, 9 Δ=1, λ=0.03, A=1,Rd=0.5

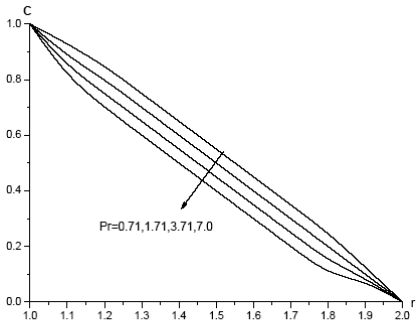

Fig.10c : Variation of C with Pr
G=2,M=2, D^{-1}=0.2,Sc=0.24, N=1, S_0=0.5,Q_1=0.5,
γ=0.5,α=2, Ec=0.01, 9 Δ=1, λ=0.03, A=1,Rd=0.5

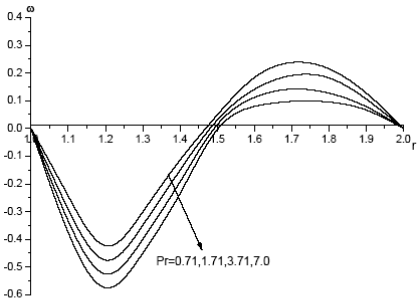

Fig.10d : Variation of ω with Pr
G=2,M=2, D^{-1}=0.2,Sc=0.24, N=1, S_0=0.5,Q_1=0.5,
γ=0.5,α=2, Ec=0.01, 9 Δ=1, λ=0.03, A=1,Rd=0.5

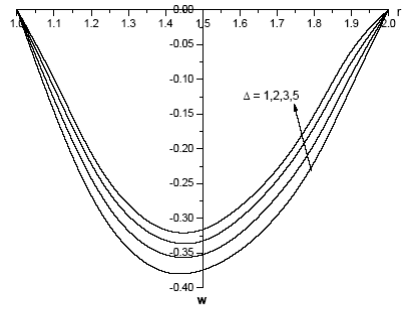

Fig. 11a : Variation of w with Δ
G=2,M=2, D^{-1}=0.2,Sc=0.24, N=1, S_0=0.5,Q_1=0.5,
γ=0.5,α=2, Ec=0.01, Pr=0.71, λ=0.03, A=1,Rd=0.5

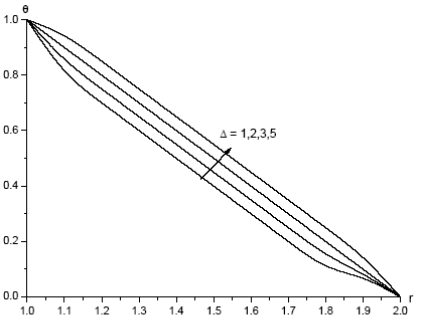

Fig. 11b : Variation of θ with Δ
G=2,M=2, D^{-1}=0.2,Sc=0.24, N=1, S_0=0.5,Q_1=0.5,
γ=0.5,α=2, Ec=0.01, Pr=0.71, λ=0.03, A=1,Rd=0.5

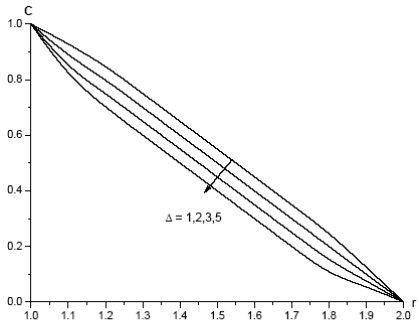

Fig. 11c : Variation of C with Δ
G=2,M=2, D^{-1}=0.2,Sc=0.24, N=1, S_0=0.5,Q_1=0.5,
γ=0.5,α=2, Ec=0.01, Pr=0.71, λ=0.03, A=1,Rd=0.5

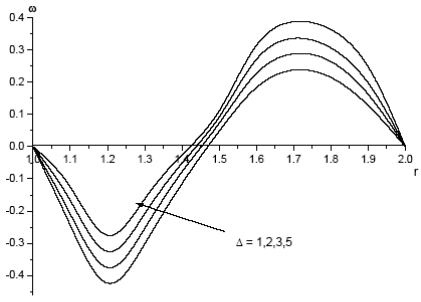

Fig. 11d : Variation of ω with Δ
G=2,M=2, D^{-1}=0.2,Sc=0.24, N=1, S_0=0.5,Q_1=0.5,
γ=0.5,α=2, Ec=0.01, Pr=0.71, λ=0.03, A=1,Rd=0.5

International Journal of Engineering Research & Technology (IJERT)
ISSN: 2278-0181
Vol. 15 Issue 02 , February - 2026

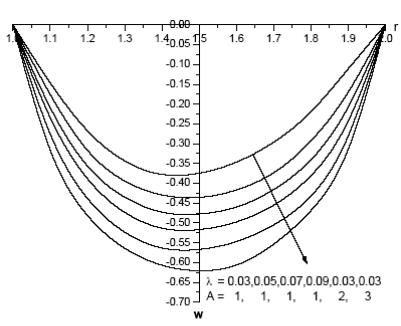

Fig. 12a : Variation of w with λ & A
G=2,M=2, D^{-1}=0.2,Sc=0.24, N=1, S_0=0.5,Q_1=0.5,
γ=0.5,α=2, Ec=0.01, Pr=0.71, Δ=1,Rd=0.5

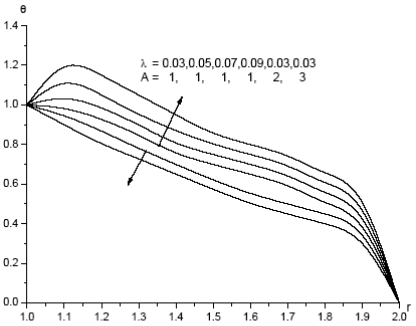

Fig. 12b : Variation of θ with λ & A
G=2,M=2, D^{-1}=0.2,Sc=0.24, N=1, S_0=0.5,Q_1=0.5,
γ=0.5,α=2, Ec=0.01, Pr=0.71, Δ=1,Rd=0.5

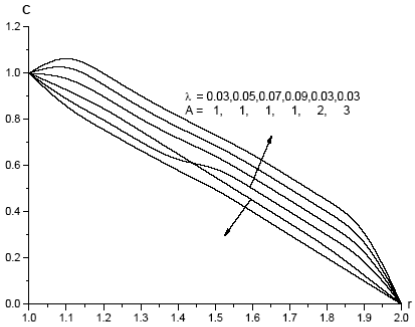

Fig. 12c : Variation of C with λ & A
G=2,M=2, D^{-1}=0.2,Sc=0.24, N=1, S_0=0.5,Q_1=0.5,
γ=0.5,α=2, Ec=0.01, Pr=0.71, Δ=1,Rd=0.5

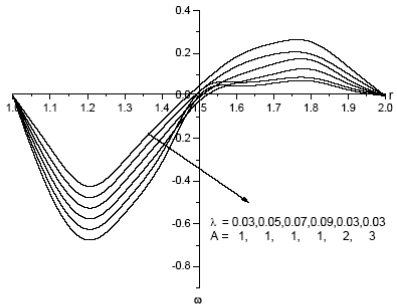

Fig. 12d : Variation of ω with λ & A
G=2,M=2, D^{-1}=0.2,Sc=0.24, N=1, S_0=0.5,Q_1=0.5,
γ=0.5,α=2, Ec=0.01, Pr=0.71, Δ=1,Rd=0.5

The rate of heat transfer (Nusselt number) (Nu) at r=1 and r=2 is shown in Tables 2&3 for different parametric values. It can be seen from the profiles that an increase in G increases |Nu| at r=1 and at r=2. The variation of Nu with M&D^{-1} shows that higher the Lorentz force /lesser the permeability of the porous medium smaller the rate of heat transfer at both the cylinders. Also |Nu| increases at r=1 and r=2 with increase in N and reduces at both the cylinders with increase in N irrespective of the directions of the buoyancy forces. An increase in suction parameter λ increases |Nu| at both cylinders. The variation of Nu with micro rotation parameter A and viscosity ratio parameter Δ shows that |Nu| reduces with Δ and A at r=1 and r=2.The variation of Nu with Ec shows that higher the dissipative heat larger |Nu| at the cylinders.Also |Nu| experiences a depreciation at r=1 &2 in degenerating and gene rating chemical reaction cases..An increase in α>0,reduces |Nu| at r=1 and r=2 with increases in the strength of the heat generating source and in the case of absorbing source it enhances at the outer cylinder and reduces at the inner cylinder r=1.Higher the thermo-diffusion effect smaller Nu at r=1 and r=2.An increase in radiation parameter (Rd) or Prandtl number (Pr) larger the rate of heat transfer at r=1&2.Also Nu reduces at r=1 and enhances at r=2 with increase in Q1..

The rate of mass transfer (Sherwood number) at r=1 and 2 is exhibited in Tables2&3 for different parametric values. It is found that the rate of mass transfer increases at r=2 and reduces at r=1 with increase in G.The rate of mass transfer em\nhances with M and decreases with D^{-1} at r =1 and at r=2 ,it reduces with M and D^{-1}.The variation of Sh with buoyancy ratio N shows that when the molecular buoyancy force dominates over the thermal buoyancy force |Sh| enhances at r=2 and reduces at r=1 when the buoyancy forces are in the same direction and for the forces acting in opposite direction it reduces at r=2 and enhances at r=1.An increase in Sc enhances Sh at r=1 and at r=2.Thus lesser the molecular diffusivity larger Sh at both the cylinders.The rate of mass transfer reduces at r=2 and enhances at r=1with increase in So.Sh reduces in the degenerating chemical reaction case and in the case of generating case,it enhances at the inner cylinder r=1 .At r=2,Sh enhances in both degenerating and generating chemical reaction cases.The rate of mass of mass transfer enhances at r=1and r=2 with increase in Q1.We find that the rate of mass transfer enhances at r=2 and reduces at r=1 with increase in suction parameter λ .The variation of Sh with Δ and A shows that Sh reduces at r=2 and enhances at r=2 with increase in Δ and A.Higher the dissipative energy smaller Sh at r=1 and r=2..An increase in the strength of the heat generating source (α>0) reduces Sh at r=1 and r=2 while in the case of heat absorbing source,Sh enhances at both the cylinders..Lesser the thermal diffusivity lesser the rate of mass transfer at the inner cylinder r=1 and larger at the outer cylinder r=2.Higher the radiative heat flux smaller Sh at r=1 and larger at r=2.

International Journal of Engineering Research & Technology (IJERT)
ISSN: 2278-0181
Vol. 15 Issue 02 , February - 2026

Table – 2
Skin friction(τ), Nusselt Number(Nu), Sherwood Number (Sh)

G	D^{-1}	N	Sc	γ	Sr	α	τ(1)	τ(2)	Nu(1)	Nu(2)	Sh(1)	Sh(2)
10	0.2	1	0.24	0.5	0.5	2	-0.0531821	0.111156	22.4196	-2.01814	22.741	-2.22309
20	0.2	1	0.24	0.5	0.5	2	-0.111573	0.225839	22.5652	-4.66668	22.6516	-4.54109
30	0.2	1	0.24	0.5	0.5	2	-0.171933	0.329391	22.7117	-6.32458	22.5781	-6.87445
10	0.4	**1**	0.24	0.5	0.5	2	-0.0525997	0.109808	22.4182	-2.00157	22.7418	-2.19987
10	0.6	1	0.24	0.5	0.5	2	-0.052344	0.109219	22.4176	-2.99434	22.7422	-2.18972
10	0.2	2	0.24	0.5	0.5	2	-0.0527152	0.100554	24.2006	-11.1775	22.1758	-12.661
10	0.2	-0.5	0.24	0.5	0.5	2	0.0966697	-0.140201	11.687	124.108	22.4286	138.135
10	0.2	-1.5	0.24	0.5	0.5	2	0.0382681	-0.0482582	20.0855	32.4642	24.4628	39.0721
10	0.2	1	0.66	0.5	0.5	2	-1.06974	2.60782	-17.616	2.67854	5.67854	70.6754
10	0.2	1	1.3	0.5	0.5	2	-1.32235	2.23397	-27.4273	52.7865	65.5643	87.6547
10	0.2	1	2.01	0.5	0.5	2	-1.56786	2.98765	-35.7865	79.7654	75.4567	98.4567
10	0.2	1	0.24	1.5	0.5	2	-0.0395013	0.0738501	24.0878	-10.3873	22.0431	-12.692
10	0.2	1	0.24	-0.5	0.5	2	-0.0882953	0.234899	20.8452	30.4695	26.7254	47.1987
10	0.2	1	0.24	-1.5	0.5	2	-0.757253	4.40273	-54.9537	76.7865	79.8975	101.6754
10	0.2	1	0.24	0.5	1.0	2	-0.0358088	0.0671503	24.183	-11.0369	22.2024	-12.4436
10	0.2	1	0.24	0.5	1.5	2	-0.0412914	0.0812704	22.9535	-8.069813	22.2862	-10.278
10	0.2	1	0.24	0.5	0.5	4	-0.0348621	0.0654007	25.1902	-19.389	22.2175	-24.3587
10	0.2	1	0.24	0.5	0.5	-2	-0.0325562	0.0678307	22.6163	1.56225	22.3942	.29791
10	0.2	1	0.24	0.5	0.5	-4	-0.0313006	0.0662402	22.3214	2.98491	22.4787	5.35571

Table – 3
Skin friction(τ), Nusselt Number(Nu), Sherwood Number (Sh)

M	Ec	Q1	Pr	Δ	λ	A		Rd	τ(1)	τ(2)	Nu(1)	Nu(2)	Sh(1)	Sh(2)
2	0.01	0.5	0.71	0.5	0.03	0.5		0.5	-0.0531821	0.111156	22.4196	-2.01814	22.741	-2.22309
5	0.01	0.5	0.71	0.5	0.03	0.5		0.5	-0.0278348	0.072688	22.3792	-2.58738	22.77	-1.61658
10	0.01	0.5	0.71	0.5	0.03	0.5		0.5	-0.0174498	0.0558291	22.3611	-2.38986	22.7825	-1.33866
2	0.03	0.5	0.71	0.5	0.03	0.5		0.5	-0.0531487	0.111146	22.4211	-2.03113	22.7387	-2.23916
2	0.05	0.5	0.71	0.5	0.03	0.5		0.5	-0.0531151	0.111135	22.4225	-2.04407	22.7364	-2.25517
2	0.01	1.0	0.71	0.5	0.03	0.5		0.5	-0.14211	0.303275	11.2132	132.157	36.2439	190.478
2	0.01	1.5	0.71	0.5	0.03	0.5		0.5	-0.203809	0.43341	-2.3420	285.837	50.3674	406.954
2	0.01	0.5	1.71	0.5	0.03	0.5		0.5	-0.0687746	0.141879	22.5860	-5.47368	22.3116	-5.82042
2	0.01	0.5	2.71	0.5	0.03	0.5		0.5	-0.11288	0.22524	22.8029	-9.36294	20.5065	-14.1231
2	0.01	0.5	7.0	0.50	0.03	0.5		0.5	-0.240291	0.463891	21.2212	12.5883	1.80865	-7.40878
2	0.01	0.5	0.71	01.0	0.03	0.5		0.5	-0.0342948	0.0501313	24.3927	-12.4164	22.0944	-16.5453
2	0.01	0.5	0.71	1.5	0.03	0.5		0.5	-0.0278598	0.00138055	24.3621	-12.9453	22.1158	-15.9235
2	0.01	0.5	0.71	0.5	0.05	0.5		0.5	-0.0287594	0.0512687	24.4112	-12.6356	22.0819	-16.8335
2	0.01	0.5	0.71	0.5	0.07	0.5		0.5	-0.0287372	0.0511787	24.4238	-12.7811	22.0732	-17.0248
2	0.01	0.5	0.71	0.5	0.03	1.0		0.5	-0.0251763	0.0538955	24.4119	-12.6751	22.0855	-16.8835
2	0.01	0.5	0.71	0.5	0.03	1.5		0.5	-0.016232	0.0657408	24.1715	-12.3012	22.3682	-15.0262
2	0.01	0.5	0.71	0.5	0.03	1.5		1.5	-0.025733	0.0462343	24.5824	-15.589	22.9128	-19.3988
2	0.01	0.5	0.71	0.5	0.03	1.5		35	-0.0224923	0.0415183	24.7732	-17.5837	22.7249	-22.0257

6. CONCLUSIONS

- An increasing in |G| enhances the axial velocity |w|, angular velocity ω and reduce the temperature θ, concentration in the entire flow region.
- Lesser the permeability of porous medium larger w, C , ω and θ in the flow region.
- The velocity ,temperature and concentration enhance,the microrotation reduces in the degenerating chemical reaction case and enhances in the generating case , the velocity enhances,temperature ,concentration and microrotation reduce in the flow region.
- An increasing suction parameter λ enhances w, θ, C and the angular velocity ω.
- The velocity and microrotation enhances and temperature ,Concentration reduces with increasing N>0 and while for N<0,the axial velocity,microrotation reduces,the the temperature and concentration enhances in the flow region.
- An increasing Eckert number Ec reduces the velocity ,temperature,concentration and microrotation.
- Higher the molecular diffusivity larger the velocity and concentration and smaller the temperature and microrotation in the flow region.

International Journal of Engineering Research & Technology (IJERT)
ISSN: 2278-0181
Vol. 15 Issue 02 , February - 2026

- An increase in heat generating source parameter ($\alpha>0$)enhances the velocity ,temperature and,microrotation and reduces the concentration while for $\alpha<0$,the velocity,the temperature enhances and theconcentration , microrotation enhance in the flow region.
- Higher the thermo-diffusion effect(or lesser the diffusion-thermo) smaller the velocity,temperature and enhances the concentration and microrotation in the flow region.
- Higher the Lorentz force smaller the stress, ans larger the rate of heat and mass transfer on the cylinders.
- An increasing $\alpha>0$ enhances $|\tau|$,$|Nu|$,$|Sh|$ enhances at r=1&2 r=1 and reduces with $\alpha<0$.
- $|\tau|$ and $|Sh|$ enhances at r=1 and r=2 with increase in Soret parameter So(or decreasing Du)
- An increasing the micropolar parameter λ enhances $|Nu|$, $|Sh|$ and $|Cw|$ at both the cylinders.
- Higher the dissipative heat smaller $|\tau|$, $|Sh|$, and larger$|Nu|$ at r=1 and 2

7. REFERENCES

[1]. Agarwal R.S. and Dhanpal C.: Numerical solution of micropolar fluid flow and heat transfer between two co-axial porous circular cylinders. Int. J. Eng. Sci., 26(11) pp. 1133-1142 (1988).
[2]. Barletta A., Magyari E., Lazzari S. and Pop I.: Closed from solutions for mixed convection with magneto hydro dynamic effect in a vertical porous annulus surrounding an electric cable. J. Heat Transfer, 131, 6, (2009).
[3]. Barletta A.: Int. J. Heat Mass Transfer, Vol. 40, pp. 15-26 (1997).
[4]. Barletta A.: Int. J. Heat Mass Transfer, Vol. 42, pp. 2243-2253, (1999).
[5]. Eringen A.C.: The theory of micropolar fluids – theory and application. Birkhauser, Bostan (1966).
[6]. El-Hakein M.A.: Int. Comns. Heat Mass Transfer, Vol. 27, pp. 581-590 (2000).
[7]. Fand R.M. and Brucker J.: Int. J. Heat and Mass Transfer. p. 723 (1986).
[8]. Grosan T., Revnic C., Pop I. and Ham D.B.: Magnetic field and internal heat generation effects on the free convection in a rectangular cavity filled with a porous medium. Int. J. Heat Mass Transfer, 52 (5-6). pp. 1525-1533(2009).
[9]. GiampietroI Fabbri: Int. J. Heat and Mass Transfer, p. 3003 (2004).
[10]. Gebhart B.J.: Fluid Mech., Vol. 14, pp. 225-232, (1962).
[11]. Gebhart B. and Mollendorf J.: Fluid Mech., Vol. 38, pp. 107 (1969).
[12]. Lukaszewicz G.: Micropolar fluids, theory and applications, Birkhauser, Bostan (1999).
[13]. Murthy D.V.S. and Singh P.: Int. J. Heat and Mass Transfer, (1997).
[14]. Murthy J.V.R. and Bahali N.K.: Steady flow of micropolar fluid through a circular pipe under a transverse magnetic field with constant suction/injection, (2009).
[15]. Nakayama A. and Pop I.: Int. Communications in Heat and Mass Transfer, (1989).
[16]. Okada K. and Ozoe H.: Experimental heat transfer rates of natural convection of molten Gallium suppressed under an external magnetic field in either the x, y or z Direction. J. Heat Transfer, 14 (1) pp. 107-114(1992).
[17]. Oreper G.M. and Szekely J.: The effect of an externally imposed magnetic field on buoyancy driven flow in a rectangular cavity. J. Crystal Growth, 64 (3), pp. 505-515, (1983).
[18]. Prasad V., Kulacki F.A. and Kulakarni A.V.: Free convection in a vertical, porous annulus with constant heat flux on the inner wall-experimental results. Int. J. Heat Mass Transfer, 29, pp. 713-723 (1986).
[19]. Panja S., Sengupta P.R. and Debnath L.: Hydro magnetic flow of Reiner – Rivlin fluid between two coaxial circular in cylinders with porous walls. Computers Math. Applic. 32 (2). pp. 1-4, (1986).
[20]. Prasad V. and Kulacki F.A.: Free convection heat transfer in a liquid-filled vertical annulus. ASME J. Heat Transfer, 107, pp. 596 (1985).
[21]. Sankar M., Venkatachalappa M. and Shivakumara I.S.: Effect of magnetic field on natural convection in a vertical cylindrical annulus. Int. J. Eng. Science, 44, pp. 1556-1570 (2006).
[22]. Shivakumara I.S., Prasanna B.M.R., Rudraiah N. and Venkatachalappa M.: Numerical study of natural convection in a vertical cylindrical Annulus using a Non-Darcy equation, J. porous Media, 5(2). pp. 87-1-2 (2002).
[23]. Shivashankar H.S., Prasanna B.M.R., Sankar M. and Sreedhara S.: Numerical study of natural convection in vertical porous Annuli in the presence of magnetic field, (2009).
[24]. Soundalgekar V.M. and Jaisawal B.S.D., Uplekar A.G. and Takhar H.S.: Appl. Mech and Engg, Vol. 4, pp. 203-218 (1999).
[25]. Sreevani M.: Mixed convective heat and mass transfer through a porous medium in channels with dissipative effects Ph.D. Thesis, S.K. University, Anantapur (A.P.), (2003).
[26]. 25a.Sulochana,C and Gnanaprasunamba,K:MHD double diffusive convective heat transfer flow of a micropolar fluid in cylindrical annulus ,International Conference in Mathematics,V.S.k.University,Bellary,Karnataka state,India(2014)
[27]. Soundalgekar V.M. and Pop I.: Int. J. Heat Mass Transfer, Vol. 17, pp. 85-90 (1974).